

Article

Pneumatic Performance Study of a High Pressure Ejection Device Based on Real Specific Energy and Specific Enthalpy

Jie Ren *, Fengbo Yang, Dawei Ma, Guigao Le and Jianlin Zhong

School of Mechanical Engineering, Nanjing University of Science and Technology, Nanjing 210094, Jiangsu, China; E-Mails: yangfengbo.cool@163.com (F.Y.); ma-dawei@mail.njust.edu.cn (D.M.); leguigao@njust.edu.cn (G.L.); njustzhongjianlin@163.com (J.Z.)

* Author to whom correspondence should be addressed; E-Mail: renjie@njust.edu.cn; Tel.: +86-25-8431-5125.

Received: 8 May 2014; in revised form: 10 August 2014 / Accepted: 29 August 2014 /

Published: 3 September 2014

Abstract: In high-pressure dynamic thermodynamic processes, the pressure is much higher than the air critical pressure, and the temperature can deviate significantly from the Boyle temperature. In such situations, the thermo-physical properties and pneumatic performance can't be described accurately by the ideal gas law. This paper proposes an approach to evaluate the pneumatic performance of a high-pressure air catapult launch system, in which residual functions are used to compensate the thermal physical property uncertainties of caused by real gas effects. Compared with the Nelson-Obert generalized compressibility charts, the precision of the improved virial equation of state is better than Soave-Redlich-Kwong (S-R-K) and Peng-Robinson (P-R) equations for high pressure air. In this paper, the improved virial equation of state is further used to establish a compressibility factor database which is applied to evaluate real gas effects. The specific residual thermodynamic energy and specific residual enthalpy of the high-pressure air are also derived using the modified corresponding state equation and improved virial equation of state which are truncated to the third virial coefficient. The pneumatic equations are established on the basis of the derived residual functions. The comparison of the numerical results shows that the real gas effects are strong, and the pneumatic performance analysis indicates that the real dynamic thermodynamic process is obviously different from the ideal one.

Keywords: thermodynamics; residual function; specific thermodynamic energy; specific enthalpy; high pressure air; compressibility factor

1. Introduction

Compared to petroleum or electric systems, high pressure air has the advantages of no pollution, high power density, cheapness, reliable performance, recycling use, and being easy to maintain [1,2]. It has been applied to industrial automation, robot driving, compressed air powered vehicles, and even some special industries such as aeronautics, astronautics, and weapons design [3]. Typically, the charging and discharging performance and exergy analysis [4] are based on the equations of state. However, in high-pressure pneumatic dynamic thermodynamic processes, the pressure is much higher than the air critical pressure and the temperature can deviate significantly from the Boyle temperature. Since the thermodynamic properties based on the ideal gas are not authentic [5], the deviations in the mass and energy balances in thermodynamic process may not be acceptable. In this paper, the specific residual thermodynamic energy and specific residual enthalpy will be derived to compensate for the real gas effect.

Extensive studies have been conducted on high pressure pneumatic systems [6,7]. In these works, most of the thermodynamic property calculations are still based on the ideal gas assumption, although the specific thermodynamic energy and specific enthalpy of an ideal gas and a real gas can differ considerably under high pressure and low temperature conditions. In this study, we will also examine the deviation between the state variables computed by the real gas equation and ideal gas assumption.

Many semi-empirical formulas have been proposed to describe the properties of real gases, including the van der Waals equation [5], Redlich-Kwong (R-K) equation [8], Soave-Redlich-Kwong (S-R-K) equation [9], Benedict-Webb-Rubin (B-W-R) equation [10], and Peng-Robinson (P-R) equation [11,12]. With the development of the corresponding states principles, these equations are applicable to all kinds of gases within a certain pressure and temperature range. However, the precision of some of these equations is not satisfactory, or when calculating the thermodynamic variables by using high order nonlinear equations, like the S-R-K and P-R equations, it will lead to the extra problem of solving transcendental equations, which appearance is not desirable. The SAFT-type equation of state [13] is accurate enough to calculate thermodynamic variables of air, while the mathematical expression of the derived functions are complex.

2. Derivation and Determination of Real Gas Equation of State for High Pressure Air

According to the corresponding state law, the compressibility factor which indicates the deviation of real gas from ideal gas can be obtained from the table of corresponding states [14]:

$$Z = \frac{PV_m}{RT} = \left(\frac{P_c V_{mc}}{RT_c} \right) \left(\frac{P_r V_{mr}}{T_r} \right) = Z_c * \varphi(P_r, T_r) \quad (1)$$

The compressibility factor is a function of the corresponding pressure and temperature. The compressibility factor value of an ideal gas is 1. For most gases, the P - Z curves can be approximately considered to be linear when the pressure $P < 0.5P_c$ or the temperature $T > 5T_c$, and the compressibility factor Z is nearly 1. However, under high pressure conditions over $0.5P_c$, or low temperature conditions below $5T_c$, a reliable and simple real gas equation of state should be derived to fit the data.

The virial coefficients which are basic thermodynamic properties represent the non-ideal behavior of real gases. The importance of the virial coefficients lies in the fact that they are related directly to the interactions between molecules. The second virial coefficient represents the deviation behavior from

ideality due to interactions between pairs of molecules, the third virial coefficient gives the effects of interactions of molecular triplets, and so on. The fourth and higher virial coefficients usually contribute little to the densities of gases and have relatively large uncertainties. Therefore, the accurate knowledge of the virial coefficients is of great significance. In order to improve the accuracy of calculation, most effort has been focused on obtaining the second [15,16] and third virial coefficients [17,18].

The volume serial form of the virial equation which is truncated to the third virial coefficient can be written as:

$$\frac{PV_m}{RT} = 1 + \frac{B}{V_m} + \frac{C}{V_m^2} \quad (2)$$

After the introduction of the critical pressure P_c , the critical temperature T_c , acentric factor ω , and the extended corresponding states variable θ [19], the second and third virial coefficients of the corresponding state can be expressed as:

$$B_r = \frac{BP_c}{RT_c} = B_r^0(T_r) + \omega B_r^1(T_r) + \theta B_r^2(T_r) \quad (3)$$

$$C_r = \frac{CP_c^2}{(RT_c)^2} = C_r^0(T_r) + \omega C_r^1(T_r) + \theta C_r^2(T_r) \quad (4)$$

where $B_r^0(T_r)$, $C_r^0(T_r)$ are obtained by fitting data for small spherical molecules ($\omega = 0$); $B_r^1(T_r)$, $C_r^1(T_r)$ are obtained from data for larger, non-spherical, non-polar molecules ($\omega \neq 0$); $B_r^2(T_r)$, $C_r^2(T_r)$ are obtained from data for non-hydrogen bonding polar molecules; and $T_r = T/T_c$.

In this paper, the real gas is assumed to be air in chemical equilibrium [20]. The National Institute of Standards and Technology (NIST) provides a basic model of air [21], which consists of nitrogen, oxygen, and argon. These are non polar molecules, the $B_r^2(T_r)$, and $C_r^2(T_r)$ of dry air are 0, and the critical parameters of air are: $T_c = 132.45\text{K}$, $P_c = 3.77\text{MPa}$. The improved formulas of $B_r^0(T_r)$, $B_r^1(T_r)$, $C_r^0(T_r)$, and $C_r^1(T_r)$ given by references [22–24] are:

$$B_r^0(T_r) = 0.13356 - \frac{0.30252}{T_r} - \frac{0.15668}{T_r^2} - \frac{0.00724}{T_r^3} - \frac{0.00022}{T_r^8} \quad (5)$$

$$B_r^1(T_r) = 0.17404 - \frac{0.15581}{T_r} + \frac{0.38183}{T_r^2} - \frac{0.44044}{T_r^3} - \frac{0.00541}{T_r^8} \quad (6)$$

$$C_r^0(T_r) = 0.01407 + \frac{0.02432}{T_r^{2.8}} - \frac{0.00313}{T_r^{10.5}} \quad (7)$$

$$C_r^1(T_r) = -0.02676 + \frac{0.0177}{T_r^{2.8}} + \frac{0.04}{T_r^3} - \frac{0.003}{T_r^6} - \frac{0.00228}{T_r^{10.5}} \quad (8)$$

The Peng-Robinson (P-R) equation, Equation (9), is an improvement on the van der Waals equation. It was proposed in 1976 [12,13]:

$$p = \frac{RT}{v-b} - \frac{a(T)}{v(v+b) + b(v-b)} \quad (9)$$

where $a(T) = 0.42748 \left(\frac{R^2 T_c^2}{p_c} \right) \left[1 + r(1 - T_r^{0.5}) \right]^2$, $r = 0.48 + 1.574w - 0.176w^2$, and $b = \frac{0.08664RT_c}{p_c}$.

In the general high pressure pneumatic system, the pressure can reach 30 MPa, and the temperature range is about $250 \text{ K} < T < 400 \text{ K}$. Compared with the Nelson-Obert’s generalized compressibility chart [1], the P-R equation is more precise than the S-R-K equation in the compressibility factor calculation of air [1]. In this paper we calculate the compressibility factor, using improved virial and P-R equations. The results of some feature points are shown in Table 1. The data for air fitted in this paper are provided by the real properties database of National Institute of Standards and Technology (NIST) [25], as shown in Table 2.

Table 1. Compressibility factors of air using improved virial equation and P-R equation.

Compressibility Factors Z		Pressure [MPa]							
		0.101	1	6	12	19.43	25	30	
Temperature [K]	400	virial	1.0002	1.0019	1.0146	1.0358	1.0695	1.0986	1.1268
		P-R	1.0001	1.0007	1.0077	1.0231	1.0504	1.0755	1.1005
	298	virial	0.9997	0.9969	0.9880	0.9922	1.0173	1.0470	1.0788
		P-R	0.9994	0.9947	0.9772	0.9773	1	1.0275	1.0620
	250	virial	0.9990	0.9907	0.9540	0.9351	0.9505	0.9832	1.0209
		P-R	0.9987	0.9875	0.9392	0.9190	0.9382	0.9725	1.0170
	200	virial	0.9976	0.9765	0.8687	0.7942	0.8133	0.8685	0.9278
		P-R	0.9970	0.9710	0.8476	0.7831	0.8157	0.8775	0.9465

Table 2. Specific volume within different temperature and pressure.

Specific volume [m ³ /kg]		Pressure [MPa]								
		0.1	0.5	1	6	10	15	20	25	30
Temperature [K]	100	0.281	0.0509	0.00130	0.00126	0.00125	0.00122	0.00120	0.00119	0.00117
	140	0.399	0.0773	0.0370	0.00222	0.00174	0.00158	0.00150	0.00144	0.00139
	200	0.537	0.114	0.0561	0.00833	0.00467	0.00309	0.00245	0.00214	0.00195
	260	0.746	0.149	0.0741	0.0120	0.00713	0.00478	0.00368	0.00307	0.00269
	300	0.861	0.172	0.0859	0.0142	0.00855	0.00578	0.00446	0.00368	0.00318
	400	0.148	0.230	0.115	0.0194	0.0118	0.00806	0.00620	0.00509	0.00437

The error results when calculating the compressibility factor within the pressure range of $0.101325 \text{ MPa} < P < 30 \text{ MPa}$ at the temperatures of 400 K, 300 K and 260 K, respectively, are shown as Table 3. From Table 3, it is found that the precision of improved virial equation is better than P-R equation compared to the NIST database.

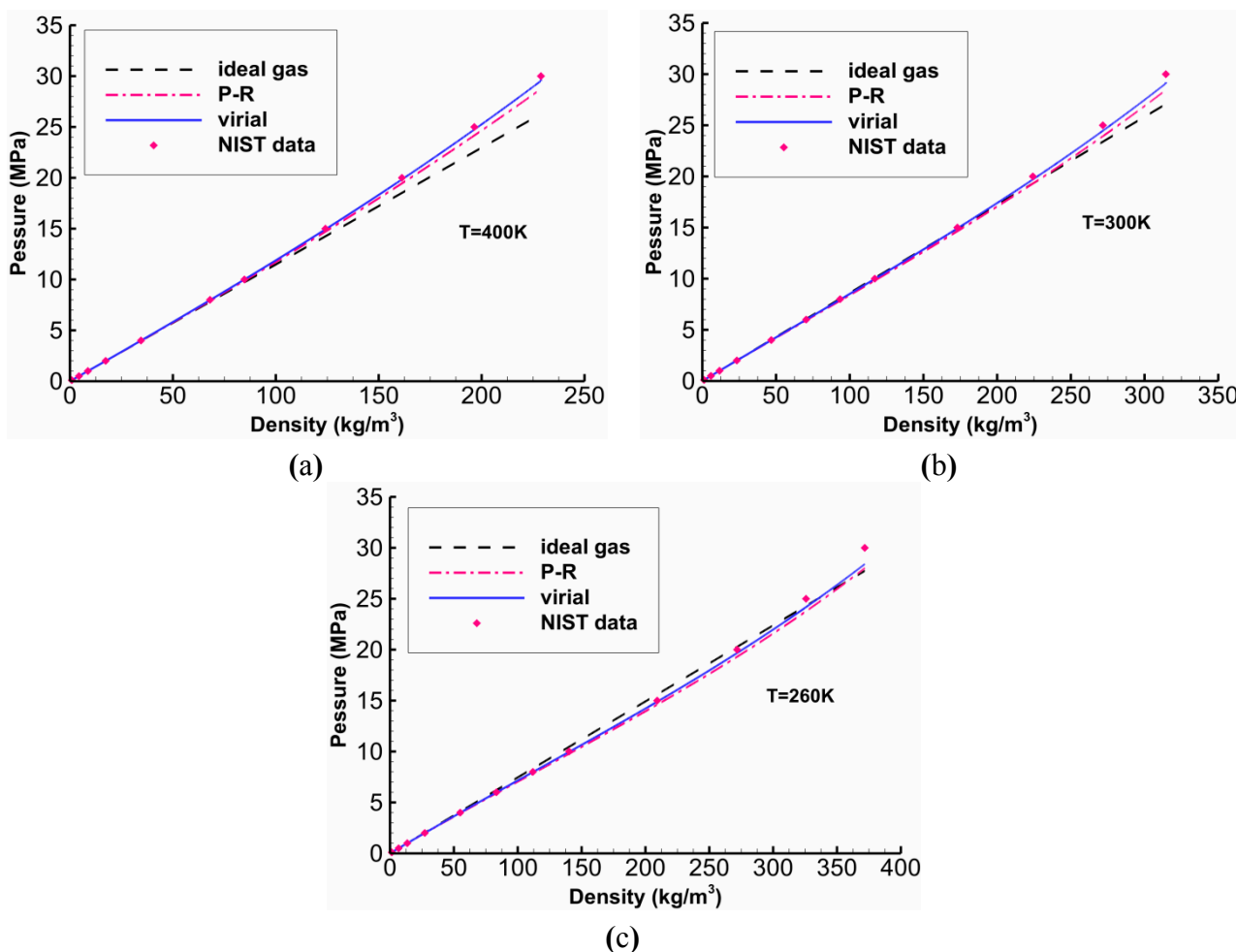
Compared with the P-R equation, the precision of the improved virial equation is better. The precision can meet the requirements of general engineering computation. Therefore, the improved virial equation is adopted to calculate compressibility factor, and in this paper the thermodynamic variables will be derived based on the improved virial equation of state.

Table 3. Error of compressibility factors for air using improved virial equation and P-R equation respectively.

Temperature [K]	Pressure range [MPa]	P-R equation		Improved virial equation	
		Maximum absolute error	Maximum relative error	Maximum absolute error	Maximum relative error
400	0.101325~30	0.0415	3.63%	0.0152	1.33%
300	0.101325~30	0.0467	4.21%	0.0274	2.47%
260	0.101325~30	0.0555	5.13%	0.0457	4.23%

Figure 1 shows the relationship between the pressure and density of high pressure air under different temperature conditions using different equations of state. It is found that the improved virial equation shows good agreement with the NIST data.

Figure 1. Comparison of real gas equations of state ($T = 400\text{ K}$, $T = 300\text{ K}$, $T = 260\text{ K}$).



3. Modeling Thermodynamic Variables

The dynamic thermodynamic analysis under high pressure conditions such as mass flow rate, charging and discharging processes, and exergy analysis in the pneumatic system are of particular interest in many applications. Therefore, to investigate the thermal behaviors in thermodynamic

processes, which can be used to predict the gas pressure, temperature and flow rate, it is essential to derive the thermodynamic variables on the basis of real gas equation states. In this section, the real analytical expressions of specific thermodynamic energy and specific enthalpy will be derived for high pressure air.

3.1. Residual Functions

In the calculation of real thermodynamic property variables, the ideal value can be calculated first, then the residual function will subtracted from the ideal value. The definition of residual function can be expressed as:

$$F_{re} = F^* - F \quad (10)$$

where F_{re} denotes the residual of a arbitrary extensive properties or specific properties, that is, the difference between the properties of ideal gas and real gas, F^* denotes the properties of ideal gas, and F denotes the properties of real gas.

The differential form of specific thermodynamic energy for real gas is:

$$du = c_v dT - [p - T\left(\frac{\partial p}{\partial T}\right)_v] dv \quad (11)$$

We have:

$$\left(\frac{\partial u}{\partial v}\right)_T = T\left(\frac{\partial p}{\partial T}\right)_v - p \quad (12)$$

The residual specific thermodynamic energy for a real gas is obtained by integrating the equation above from $v^* = \infty$ (ideal gas state) to v (real gas state) along the isotherm:

$$u_r = \int_{\infty}^v \left[p - T\left(\frac{\partial p}{\partial T}\right) \right] dv = -T^2 \int_{\infty}^v \left[\frac{\partial(p/T)}{\partial T} \right] dv \quad (13)$$

The specific enthalpy for a real gas is defined as:

$$h = u + pv \quad (14)$$

and the specific enthalpy for an ideal gas can be expressed by:

$$h^* = u^* + R_g T \quad (15)$$

Combination of the above three equations will lead to:

$$h_r = -T^2 \int_{\infty}^v \left[\frac{\partial(p/T)}{\partial T} \right] dv - pv + R_g T \quad (16)$$

3.2 Thermodynamic Variables of Ideal Gas

The specific thermodynamic energy and specific enthalpy of ideal gas can be written as:

$$u^*(T) = \int_{T_0}^T c_v^* dT + u_0 \quad (17)$$

$$h^*(T) = \int_{T_0}^T (c_V^* + R_g) dT + h_0 \tag{18}$$

For ideal gas, isochoric heat capacity can be expressed by:

$$c_V^* = R_g \left((\alpha - 1) + \beta T + \gamma T^2 + \delta T^3 + \varepsilon T^4 \right) \tag{19}$$

where $\alpha = 3.653$, $\beta = -1.337 \times 10^{-3}$, $\gamma = 3.294 \times 10^{-6}$, $\delta = -1.913 \times 10^{-9}$, and $\varepsilon = 0.2763 \times 10^{12}$.

3.3 Thermodynamic Variables of Real Gas

Based on the improved virial equation and substituting Equations (13), (16), (17) and (18) into Equation (10), respectively, the analytical expressions of specific thermodynamic energy and specific enthalpy for real gas are obtained as follows:

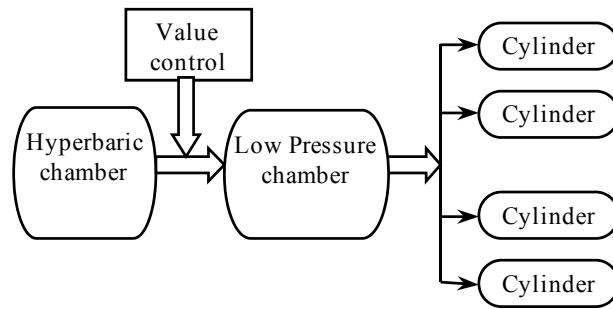
$$\begin{aligned}
 u = & \int_{T_0}^T \left(R_g \left((\alpha - 1) + \beta T + \gamma T^2 + \delta T^3 + \varepsilon T^4 \right) \right) dT + u_0 \\
 & - \left[\frac{RR_g T_c}{p_c V_m} \left(0.30252 T_c + \frac{0.31336 T_c^2}{T} + \frac{0.02172 T_c^3}{T^2} + \frac{0.00176 T_c^8}{T^7} \right. \right. \\
 & \quad \left. \left. + w \left(0.15581 T_c - \frac{0.763662 T_c^2}{T} + \frac{1.32132 T_c^3}{T^2} + \frac{0.04328 T_c^8}{T^7} \right) \right) \right] \\
 & + \frac{R^2 R_g T_c^2}{2 p_c^2 V_m^2} \left(- \frac{0.068096 T_c^{2.8}}{T^{1.8}} + \frac{0.032865 T_c^{10.5}}{T^{9.5}} + w \left(- \frac{0.04956 T_c^{2.8}}{T^{1.8}} - \frac{0.12 T_c^3}{T^2} + \frac{0.018 T_c^6}{T^5} + \frac{0.02394 T_c^{10.5}}{T^{9.5}} \right) \right) \tag{20}
 \end{aligned}$$

$$\begin{aligned}
 h = & \int_{T_0}^T \left(R_g \left(\alpha + \beta T + \gamma T^2 + \delta T^3 + \varepsilon T^4 \right) \right) dT + h_0 - \\
 & - \left[\frac{RR_g T_c}{p_c V_m} \left(0.30252 T_c + \frac{0.31336 T_c^2}{T} + \frac{0.02172 T_c^3}{T^2} + \frac{0.00176 T_c^8}{T^7} \right. \right. \\
 & \quad \left. \left. + w \left(0.15581 T_c - \frac{0.763662 T_c^2}{T} + \frac{1.32132 T_c^3}{T^2} + \frac{0.04328 T_c^8}{T^7} \right) \right) \right] \\
 & + \frac{R^2 R_g T_c^2}{2 p_c^2 V_m^2} \left(- \frac{0.068096 T_c^{2.8}}{T^{1.8}} + \frac{0.032865 T_c^{10.5}}{T^{9.5}} + w \left(- \frac{0.04956 T_c^{2.8}}{T^{1.8}} - \frac{0.12 T_c^3}{T^2} + \frac{0.018 T_c^6}{T^5} + \frac{0.02394 T_c^{10.5}}{T^{9.5}} \right) \right) \tag{21} \\
 & + R_g T \left(\frac{RT_c (B_r^0(T_r) + \omega B_r^1(T_r) + \theta B_r^2(T_r))}{v M P_c} + \frac{(RT_c)^2 (C_r^0(T_r) + \omega C_r^1(T_r) + \theta C_r^2(T_r))}{v^2 M^2 P_c^2} \right)
 \end{aligned}$$

4. Modeling of Pneumatic Catapult

Figure 2 shows the working principle of a high pressure pneumatic catapult, and Figure 3 is the schematic diagram of the lifting ejection mechanism which is a schematic structural diagram of the three-step piston cylinder in Figure 1 and component 6 in Figure 4. There d_a is the diameter of the piston rod, d_c is the diameter of piston, S_a is an effective thrust area of the third stage cylinder, L_b represents the second cylinder, and L_c represents the third stage cylinder.

Figure 2. High pressure gas supply system.



The working principle of the lifting ejection system can be described as follows: as the launching process starts, the controlled valve immediately responds and opens, and high-pressure gas flows into the low pressure chamber; the second stage of the cylinder pushes the piston to move forward, then the first stage of the cylinder pushes the piston to move forward after the second stage moves to the end; missile moves with lifting beam, then lifting beam collides with the buffer, and missile flies out of the launch tube.

In the course of the pneumatic ejection, taking the subsonic and sonic flow into account, mass flow equation can be written as:

$$G_c = \begin{cases} \mu_x \frac{p_1 A}{\sqrt{R_g T_1}} \sqrt{\frac{2k}{k-1} \left[\left(\frac{p_2}{p_1}\right)^{\frac{2}{k}} - \left(\frac{p_2}{p_1}\right)^{\frac{k+1}{k}} \right]}, & \left(\frac{2}{k+1}\right)^{\frac{k}{k-1}} < \frac{p_2}{p_1} < 1 \\ \mu_x \sqrt{k} \left(\frac{2}{k+1}\right)^{\frac{k+1}{2(k-1)}} p_1 A / \sqrt{R_g T_1}, & \frac{p_2}{p_1} \leq \left(\frac{2}{k+1}\right)^{\frac{k}{k-1}} \end{cases} \quad (22)$$

where subscripts 1 and 2 indicate high-pressure chamber and low pressure chamber respectively, μ_x is flow correction factor, A denotes the equivalent cross-sectional area of orifice, and k denotes the adiabatic index.

According to mass and energy conservation laws, and the flow equation in the high-pressure chamber and low pressure chamber, the following relations can be established:

$$\begin{cases} \frac{d}{dt}(\rho_1 V_1) = -Q_m \\ \frac{d}{dt}(\rho_1 V_1 u_1) = -Q_m h_1 \\ p_1 = \frac{RT_1}{V_{m1}} \left(1 + \frac{B_1}{V_{m1}} + \frac{C_1}{V_{m1}^2}\right) \\ \frac{dm_2}{dt} = Q_m \\ \frac{d}{dt}(m_2 u_2) = Q_m h_1 - n s_t p_2 \frac{dl}{dt} \\ m_e \frac{dv_2}{dt} = n(p_2 - p_a) s_t - 1.2 m_e g \sin(\alpha) \\ p_2 = \frac{RT_2}{V_{m2}} \left(1 + \frac{B_2}{V_{m2}} + \frac{C_2}{V_{m2}^2}\right) \end{cases} \quad (23)$$

where m_e is the quality of missile, P_a denotes the atmospheric pressure, g is the acceleration of gravity, v_2 is the speed of missile, and s_t denotes effective thrust area.

Let $X_1=\rho_1, X_2=T_1, X_3=m_2, X_4=T_2, X_5=l, X_6=v_2$, the closed pneumatic equations can be established as:

$$\begin{cases}
 \dot{X}_1 = -G_c / V_1 \\
 \dot{X}_2 = \frac{-G_c \left\{ \left[\frac{R_g RT_c}{p_c V_{m1}} D_{111} \left(1 + \frac{M_0}{X_1 V_{m1}} \right) + \frac{R_g R^2 T_c^2}{p_c^2 V_{m1}^2} D_{121} \left(\frac{1}{2} + \frac{M_0}{X_1 V_{m1}} \right) \right] - \int_{298.15}^{X_2} c_v^* dT - u_0 \right\} - G_c (h_1^* - h_{1r}) / V_1}{X_1 \left[c_v^* - \frac{R_g RT_c}{p_c V_{m1}} D_{211} - \frac{R_g R^2 T_c^2}{2 p_c^2 V_{m1}^2} D_{221} \right]} \\
 \dot{X}_3 = G_c \\
 \dot{X}_4 = \left\{ \left[\int_{298.15}^{X_4} c_v^* dT + e - \left(\frac{R_g RT_c}{p_c V_{m2}} D_{112} + \frac{R_g R^2 T_c^2}{2 p_c^2 V_{m2}^2} D_{122} \right) - \frac{R_g RT_c M_0 (V_0 + ns_0 X_5)}{p_c V_{m2}^2 X_3} \left(1 + \frac{RT_c}{p_c V_{m2}} \right) - (h_1^* - h_{1r}) \right] G_c \right. \\
 \left. + ns_0 p_2 X_6 + \frac{R_g RT_c M_0 ns_0 X_6}{p_c V_{m2}^2} \left(1 + \frac{RT_c}{p_c V_{m2}} \right) \right\} / \left[-X_3 c_v^* + \frac{X_3 R_g RT_c}{p_c V_{m2}} D_{212} + \frac{X_3 R_g R^2 T_c^2}{2 p_c^2 V_{m2}^2} D_{222} \right] \\
 \dot{X}_5 = X_6 \\
 \dot{X}_6 = \begin{cases} \frac{n(p_2 - p_0)s_0 - 1.2M_0g \sin(\alpha)}{M_0}, & p_2 \geq p_0 + 1.2 \frac{M_0g \sin(\alpha)}{ns_0} \\ 0, & p_2 < p_0 + 1.2 \frac{M_0g \sin(\alpha)}{ns_0} \end{cases} \\
 D_{211} = \frac{-0.31336T_c^2}{X_2^2} - \frac{0.04344T_c^3}{X_2^3} - \frac{0.01232T_c^8}{X_2^8} + \omega \left(\frac{0.763662T_c^2}{X_2^2} - \frac{2.64264T_c^3}{X_2^3} - \frac{0.30296T_c^8}{X_2^8} \right) \\
 D_{221} = \frac{0.1225728T_c^{2.8}}{X_2^{2.8}} - \frac{0.3122175T_c^{10.5}}{X_2^{10.5}} + \omega \left(\frac{0.089208T_c^{2.8}}{X_2^{2.8}} + \frac{0.24T_c^3}{X_2^3} - \frac{0.09T_c^6}{X_2^6} - \frac{0.22743T_c^{10.5}}{X_2^{10.5}} \right) \\
 D_{112} = 0.30252T_c + \frac{0.31336T_c^2}{X_4} + \frac{0.02172T_c^3}{X_4^2} + \frac{0.00176T_c^8}{X_4^7} \\
 + \omega \left(0.15581T_c - \frac{0.763662T_c^2}{X_4} + \frac{1.32132T_c^3}{X_4^2} + \frac{0.04328T_c^8}{X_4^7} \right) \\
 D_{122} = -\frac{0.068096T_c^{2.8}}{X_4^{1.8}} + \frac{0.032865T_c^{10.5}}{X_4^{9.5}} + \omega \left(-\frac{0.04956T_c^{2.8}}{X_4^{1.8}} - \frac{0.12T_c^3}{X_4^2} + \frac{0.018T_c^6}{X_4^5} + \frac{0.02394T_c^{10.5}}{X_4^{9.5}} \right) \\
 D_{212} = \frac{-0.31336T_c^2}{X_4^2} - \frac{0.04344T_c^3}{X_4^3} - \frac{0.01232T_c^8}{X_4^8} + \omega \left(\frac{0.763662T_c^2}{X_4^2} - \frac{2.64264T_c^3}{X_4^3} - \frac{0.30296T_c^8}{X_4^8} \right) \\
 D_{222} = \frac{0.1225728T_c^{2.8}}{X_4^{2.8}} - \frac{0.3122175T_c^{10.5}}{X_4^{10.5}} + \omega \left(\frac{0.089208T_c^{2.8}}{X_4^{2.8}} + \frac{0.24T_c^3}{X_4^3} - \frac{0.09T_c^6}{X_4^6} - \frac{0.22743T_c^{10.5}}{X_4^{10.5}} \right)
 \end{cases} \tag{24}$$

Figure 3. Three-step piston cylinder simplified diagram.

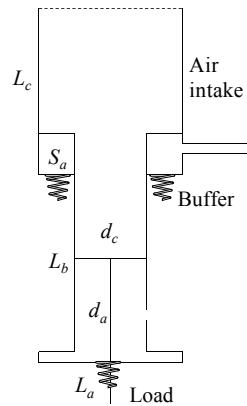
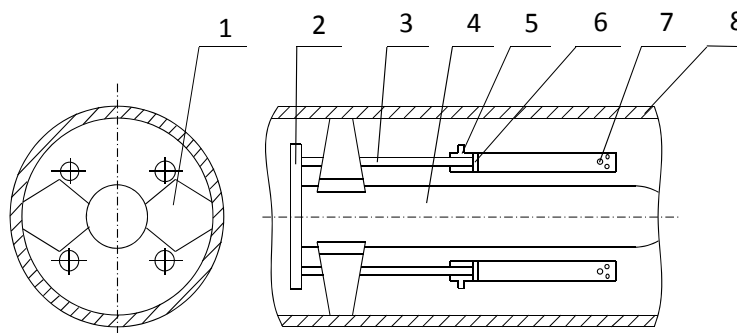


Figure 4. Lifting ejection mechanism sketch.



- 1-folding wing, 2-lifting beam, 3-lifting pole, 4-missile,
- 5-gas inlet, 6-three-step piston cylinder, 7-exhaust orifice,
- 8-launch tube.

5. Simulation Analysis of the Pneumatic Ejection

The system parameters of above mathematical model and thermo-physical parameters are as shown in Table 4. The five-step four-order Runge-Kutta method is used to calculate the pneumatic ejection process based on ideal gas equation and real gas equation respectively. The basic idea of five-step four-order Runge-Kutta method is expressed as:

$$\begin{cases}
 k_{i1} = f_i(t_j, X_{1j}, \dots, X_{6j}) \\
 k_{i2} = f_i\left(t_j + \frac{t_0}{2}, X_{1j} + \frac{t_0 k_{i1}}{2}, \dots, X_{6j} + \frac{t_0 k_{i1}}{2}\right) \\
 k_{i3} = f_i\left(t_j + \frac{t_0}{2}, X_{1j} + \frac{t_0 k_{i2}}{2}, \dots, X_{6j} + \frac{t_0 k_{i2}}{2}\right), \quad i = 1, 2, \dots, 6 \\
 k_{i4} = f_i(t_j + t_0, X_{1j} + t_0 k_{i3}, \dots, X_{6j} + t_0 k_{i3}) \\
 X_{i,j+1} = X_{i,j} + t_0 \left(\frac{k_{i1}}{6} + \frac{k_{i2}}{3} + \frac{k_{i3}}{3} + \frac{k_{i4}}{6}\right)
 \end{cases} \quad (25)$$

where t_0 indicates time step, and j represents the current time step.

Table 4. System parameters and thermal physical parameters of dry air.

Parameters	Values
Universal gas constant R [J/mol·K]	8.3145
Critical temperature T_c [K]	132.45
Critical pressure P_c [MPa]	3.77
Acentric Factor ω	0.031
Gas constant of air R_g [J/kg·K]	287.0
Molar mass M [g/mol]	28.97
Flow correction factor μ_x	0.95
Cross-sectional area valve control A [m ²]	0.0123
Adiabatic index k	1.4
Initial gas density of “1” ρ_1 [kg/m ³]	360
Initial gas temperature of “1” T_1 [K]	300
Volume of “1” V_1 [m ³]	1.8
Initial gas mass of “2” m_2 [kg]	26
Initial gas temperature of “2” T_2 [K]	300
The number three piston cylinder n	4
Effective thrust area of cylinder S_0 [m ²]	0.0235
Mass of missile M_0 [kg]	24,000
Launch angle α [deg]	90
Initial volume of “2” V_0 [m ³]	0.7

5.1. Comparative Analysis of Dynamic Thermodynamic Processes

Figures 5–9 show the dynamic variation comparison of the main thermodynamic variables in the ejection process. When air flows from high pressure chamber to low pressure chamber in the throttling process, the temperature will change with the pressure drop. The throttling process is assumed to be an isenthalpic process. From Figure 5, we can see that the high pressure air flows into the low pressure chamber, the temperature in the high pressure chamber decreases all the time. In the initial stage, the temperature of the low-pressure chamber increases immediately, and then decreases gradually when the missile moves upward. Also, from Figure 5, we can see that the real temperature in the high chamber decreases faster than the ideal temperature before 0.2 s. This can be explained from the following two aspects: firstly, Figure 9 shows that the gas mass based on real gas and ideal gas flowing into the low pressure chamber are nearly equal; secondly, Figure 7 shows that the residual enthalpy in high pressure chamber is positive, the real enthalpy of high pressure air is obviously less than ideal one. As a result, the real temperature in the high chamber decreases faster before 0.2 s.

From Figure 5, we know the temperature in the low pressure chamber increases immediately, and then decreases slowly when the missile moves upward. It shows that the real temperature of gas in the low pressure is always lower than ideal one, which indicates that the real gas effects decelerates the temperature increasing rates in the low pressure chamber in the early stage, and accelerates the rate of decrease of the temperature with the missile moving upward.

Figure 6 shows the pressure variations in the high pressure chamber and low pressure chamber. We can see that the hyperbaric always deflates, and the pressure continues to decay. High pressure air flows into low pressure chamber that the pressure in the low pressure chamber increases before the missile

starts to move, and decreases as the missile moves upward. The real pressure decay rate is greater than the ideal decay rate. This is due to the following facts: firstly, from the analysis above, we know that the real temperature in the high chamber decreases faster than the ideal one; secondly, the real gas mass flowing out of high pressure chamber is nearly the same as the ideal mass. The first factor is the dominant factor which makes the phenomenon happened. The ideal value of temperature in the hyperbaric pressure chamber is much greater than the actual value which is similar to low pressure chamber.

Figure 5. Temperature contrast curve.

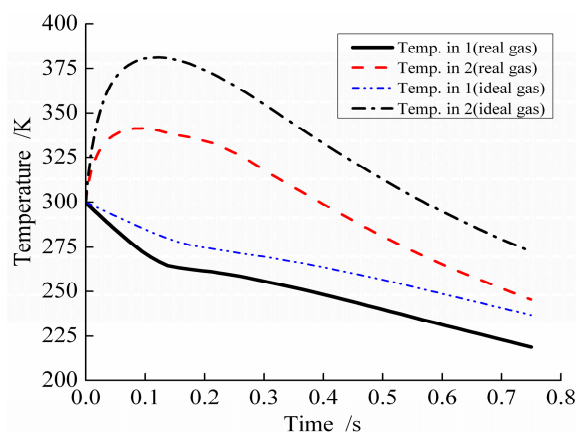
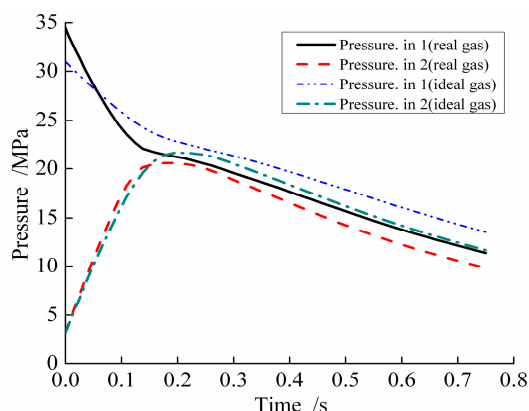


Figure 6. Pressure contrast curve.



From Figure 7, we can see that the specific enthalpy in the hyperbaric chamber increases first and then decreases slightly, while the specific enthalpy in the low pressure chamber rises rapidly, and then increases slowly. When the pressure getting higher, the distance between molecules becomes smaller and the intermolecular interaction becomes stronger, as a result, the specific enthalpy gets larger and it deviates more from the ideal gas state. While the temperature increases, the situation is totally different: longer distance between molecules makes the intermolecular forces smaller, so the specific enthalpy gets smaller and it is more close to the ideal gas state. For the high pressure chamber, with gas flowing into low pressure chamber, pressure decays, and temperature decreases rapidly. Figure 7 shows the specific enthalpy in the high pressure chamber drops slightly, which indicates that the pressure drop is the main factor. For the low pressure chamber, the pressure and temperature increase first, and decrease with the gas pushing the missile upwards. Figure 7 shows the specific enthalpy in the low pressure chamber increases rapidly first and then increases slightly, which indicates that the pressure increase is the main factor in the early stage, and the temperature decrease is the main factor in the later round.

Figure 7. The residual enthalpy curve.

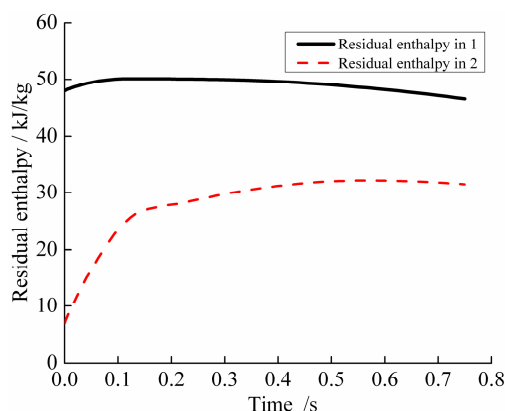


Figure 8 shows the dynamic variation of pressure compression factors in the hyperbaric chamber and low pressure chamber. The maximum compression factor reaches 1.1013 and 1.0486, respectively. From Equation (1) we can see that the compressibility factor is determined by temperature and pressure. As shown in Figure 5 and Figure 8, the compressibility factor variation law is similar to the pressure one which indicates that the pressure dominates the changing regulation of the compression factor.

Figure 8. The compressibility factor curve.

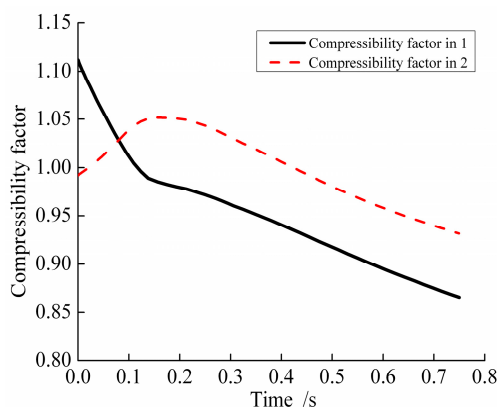
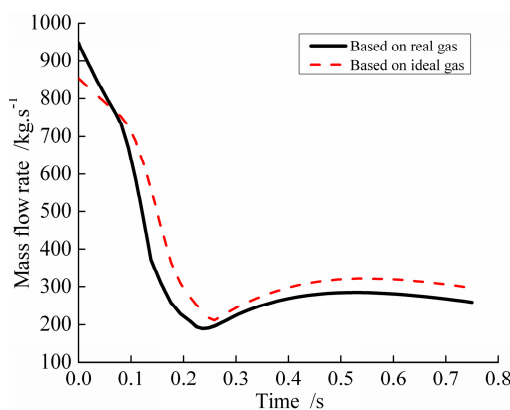


Figure 9 shows the mass flow rate declines rapidly at first, and then rises slowly. It is also noticed in Figure 9 that the real gas effect accelerates the rate of decrease of the mass flow in the early stage, and decelerates the rates of increase in the later period.

Figure 9. The mass flow rate curve.



5.2. Ejection Performance Evaluation Variables

With the missile overload consistent with the pressure in the low pressure chamber, agreement between the acceleration of missile and pressure in the low pressure chamber are fairly satisfied, regardless of whether the correspondence relationship is based on a real gas or based on an ideal gas, just as shown in Figures 5 and 9.

The missile speed is a linear function of acceleration, and the missile stroke is a quadratic function of acceleration, while the ejection time is less than 1 s. It is shown that the velocity of missile based on an ideal gas is significantly greater than that based on a real gas, and missile stroke based on an ideal gas is slightly larger than that based on a real gas shown in Figures 10–12.

Figure 10. The acceleration curves.

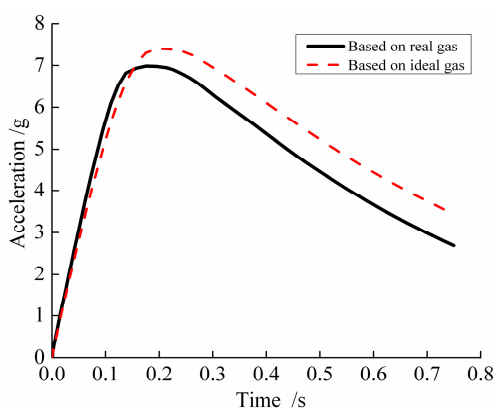


Figure 11. The velocity curve.

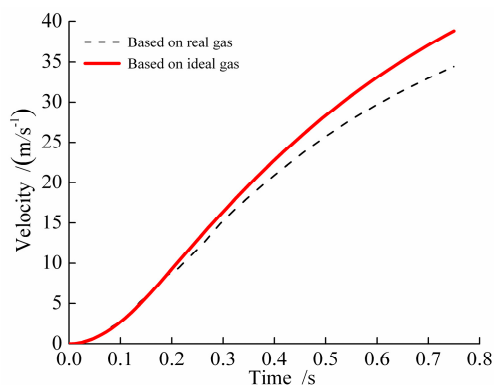
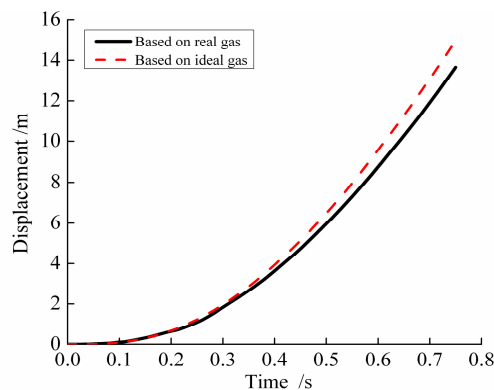


Figure 12. The displacement curve.



6. Conclusions

In this paper, the improved virial equation of state is used to describe the thermodynamic properties of high pressure air by fitting the NIST data. The compressibility factor is utilized to evaluate the precision of the equation of state. Compared with the NIST data, the compressibility factor value obtained from the improved virial equation has a maximum error of 1.33%, 2.47% and 4.23% within the pressure ranges of $0.101325 \text{ MPa} < P < 30 \text{ MPa}$ at the temperatures of 400 K, 300 K and 260 K, respectively, and the precision of the improved virial equation of state is better than that of the existing P-R and S-R-K equations.

Also, the analytical expression for thermodynamic variables, such as the specific residual thermodynamic energy and specific residual enthalpy are presented to compensate the real gas effects, based on the improved virial equation of state. The study on dynamic thermodynamic analyses, mass flow rate, charging and discharging processes, and exergy analysis are of particular importance in high pressure air applications. In addition, based on the real thermodynamic variables, the internal ballistics mathematical model for a pneumatic ejection system is established, with the real gas effects considered. Numerical simulations are also performed.

The detailed dynamic thermodynamic processes for discharging processes in the hyperbaric chamber and charging processes in the low pressure chamber are analyzed. The comparison of the numerical results indicate that the value of residual enthalpy is high, the state of the working fluid deviates from the ideal gas, and the compressibility of working fluid is strong, as the compression factor reaches 1.107. The real gas effects accelerate the pressure and temperature rates of decrease in the hyperbaric pressure chamber, and decelerate the rates of increase in the low pressure chamber.

Acknowledgments

The authors acknowledge the support from the National Natural Science Foundation of China (Grant No. 51303081) and the Natural Science Foundation of Jiangsu Province, China (Grant No. BK20130761).

Authors Contributions

Dawei Ma conceived of the ideal that we can apply high pressure ejection device to weapon scope in line with the development direction for new concept weapons. His main contribution is the problem motivation. Jie Ren established the structure scheme of the high pressure pneumatic catapult, and developed the method to evaluate the real gas effects, by establishing compression factor library. Jie Ren also deduced the closed pneumatic equations to analyse the real dynamic thermodynamic process, by presenting the analytical expressions of specific residual thermodynamic energy and specific residual enthalpy of the high-pressure air based on real gas state equation. Fengbo Yang developed the research program to study the real gas effects, by using five-step four-order Runge-Kutta method to solve the closed pneumatic equations and calculated the compression factor based on P-R equation and improved virial equation. The contribution of Jianlin Zhong was to deduce the closed pneumatic equations based on ideal gas, including the mass and energy conservation laws. Guigao Le was responsible for the comparative analysis of the pneumatic catapult performance based on real gas state equation and ideal

gas state equation, including the analysis of dynamic thermodynamic processes and article polish. All authors have read and approved the final manuscript.

Nomenclature

Z	compressibility factor, dimensionless	h	specific enthalpy, J/kg
P	pressure, MPa	R_g	gas constant, J/(kg·K)
T	temperature, K	s	specific entropy, J/(kg·K)
V_m	molar volume, m ³ /mol	$\alpha, \beta, \gamma, \delta, \varepsilon$	constants
R	universal gas constant, J/(mol·K)	ρ	density, (kg/m ³)
B	the second virial coefficient, dimensionless	n	polytropic exponent, dimensionless
C	the third virial coefficient, dimensionless	Subscripts	
ω	acentric factor, dimensionless	r	corresponding value
Θ	extended corresponding states variables, dimensionless	c	critical value
u	specific thermodynamic energy, J/kg	re	residual value
C_v	isochoric heat capacity, J/(kg·K)	*	ideal gas
v	specific volume, m ³ /kg	0	reference state

Conflict of Interest

The authors declare no conflict of interest.

References

1. Luo, Y.; Wang, X. Exergy analysis on throttle reduction efficiency based on real gas equations. *Energy* **2010**, *35*, 181–187.
2. Zhu, J.; Lei, J.; Huang, Z.; Fu, T. Pneumatic position servo control system based on grey relational compensation control. *Chin. J. Mech. Eng.* **2012**, *48*, 159–167. (In Chinese)
3. Wang, X.; Luo, Y.; Xu, Z. Study of polytropic exponent based on high pressure switching expansion reduction. *J. Therm. Sci.* **2011**, *5*, 435–441.
4. Yang, J.L.; Ma, Y.T.; Li, M.X.; Guan, H.Q. Exergy analysis of transcritical carbon dioxide refrigeration cycle with an expander. *Energy* **2005**, *30*, 1162–1175.
5. Chen, Z. *Advanced Engineering Thermodynamics*; Higher Education Press: Beijing, China, 2008.
6. Jia, G.; Wang, X.; Liu, H.; Wu, G. Study on pressure reduction and power property of high pressure pneumatic system on the compressed air powered vehicle. *China Mech. Eng.* **2004**, *15*, 1294–1297. (In Chinese)
7. Yang, G.; Guo, J.; Li, B. Dynamic simulation investigation of a novel high-pressure pneumatic proportional control valve. *China Mech. Eng.* **2007**, *18*, 1418–1420. (In Chinese)
8. Privat, R.; Privat, Y.; Jaubert, J.-N. Can cubic equations of state be recast in the virial form? *Fluid Phase Equilib.* **2009**, *282*, 38–50.
9. Jaubert, J.-N.; Privat, R. Relationship between the binary interaction parameters (k_{ij}) of the Peng–Robinson and those of the Soave–Redlich–Kwong equations of state: Application to the definition of the PR2SRK model. *Fluid Phase Equilib.* **2010**, *295*, 26–37.
10. Scalise, O.H. On the phase equilibrium stockmayer fluids. *Fluid Phase Equilib.* **2007**, *253*, 171–175.

11. Brown, J.S. Predicting performance of refrigerants using the Peng-Robinson equation of state. *Int. J. Refrig.* **2007**, *30*, 1319–1328.
12. Avaullee, L.; Trassy, L.; Neau, E.; Jaubert, J. Thermodynamic modeling for petroleum fluids. I. Equation of state and group contribution for the estimation of thermodynamic parameters of heavy hydrocarbons. *Fluid Phase Equilibr.* **1997**, *139*, 155–170.
13. Privat, R.; Gani, R.; Jaubert, J.N. Are safe results obtained when the PC-SAFT equation of state is applied to ordinary pure chemicals? *Fluid Phase Equilibr.* **2010**, *295*, 76–92.
14. Bi, M.; Feng, D.; Ma, L. *Engineering Thermodynamics*; Chemical Industry Press: Beijing, China, 2008. (In Chinese)
15. Scott, D.J.; Patel, T.R.; Winzor, D.J. A Potential for overestimating the absolute magnitudes of second virial coefficients by small-angle X-ray scattering. *Anal. Biochem.* **2013**, *435*, 158–165.
16. Winzor, D.J.; Scott, D.J.; Wills, P.R. A simpler analysis for the measurement of second virial coefficients by self-interaction chromatography. *Anal. Biochem.* **2007**, *371*, 21–25.
17. Ramos-Estrada, M.; Iglesias-Silva, G.A.; Hall, K.R.; Kohler, F. Estimation of third virial coefficients at low reduced temperatures. *Fluid Phase Equilibria.* **2006**, *240*, 179–185.
18. Chen, H.; Zheng, J.; Xu, P.; Li, L.; Liu, Y.; Bie, H. Study on real-gas equations of high pressure hydrogen. *Int. J. Hydrog. Energy* **2010**, *35*, 3100–3104.
19. Xiang, H. *Thermal Physical and Chemical Properties of the Fluid: The Corresponding State Principle and Application*; Science Press: Beijing, China, 2003. (In Chinese)
20. Kameyama, H.; Yoshida, K.; Yamauchi, S.; Fueki, K. Evaluation of reference exergies for the elements. *Appl. Energy* **1982**, *11*, 69–83.
21. Lemmon, E.W.; Jacobsen, R.T.; Penoncello, S.G.; Friend, D.G. Thermodynamic properties of air and mixtures of nitrogen argon and oxygen from 60 to 2000 K at pressure to 2000 MPa. *J. Phys. Chem. Ref. Data* **2000**, *29*, 331–385.
22. Chueh, P.L.; Prausnitz, J.M. Third virial coefficients of nonpolar gases and their mixtures. *AIChE J.* **1967**, *13*, 896–902.
23. Meng, L.; Duan, Y.-Y.; Wang, X.-D. Binary interaction parameter kij for calculating the second cross-virial coefficients of mixtures. *Fluid Phase Equilibr.* **2007**, *260*, 354–358.
24. Meng, L.; Duan, Y.-Y.; Li, L. Correlations for second and third virial coefficients of pure fluids. *Fluid Phase Equilibr.* **2004**, *226*, 109–120.
25. Green, D.W.; Perry, R.H. *Perry's Chemical Engineers' Handbook*, 8th ed.; McGraw-Hill Professional: New York, NY, USA, 2007.